Energy &
Environment Nexus

Original Research

Open Access

https://doi.org/10.48130/een-0025-0006

Early establishment of native halophytic plant species enhanced mineral weathering and organic carbon inputs in bauxite residue under field conditions

Songlin Wu[1], Fang You[1], Lars Thomsen[2], David Parry[3] and Longbin Huang[1*]

Received: 26 June 2025

Revised: 25 July 2025

Accepted: 14 August 2025

Published online: 24 September 2025

Abstract

The early colonizers of tolerant native plant species are important biological drivers in soil formation through rhizosphere-driven mineral weathering and *in situ* inputs of organic carbon to generate organo-mineral association and aggregation. The present study aims to investigate whether native halophytic plant species could be used as early colonizers in the surface layer of seawater-treated bauxite residue (BR), to initiate weathering of alkaline minerals and *in situ* inputs of organic carbon, when large volumes of organic matter are infeasible under field conditions. In a three-year field trial, three halophytic plant species (i.e., Ruby saltbush *Enchylaena tomentosa var. glabra*, saltbush *Atriplex aminocola,* and Rhodes grass *Chloris gayana*) were grown from seeds in the surface layer for nearly three years under field conditions. The X-ray diffraction (XRD) analysis revealed that plant establishment significantly reduced the abundance of sodalite-like minerals from over 10% to between 5%–7%, coinciding with pH reduction from 9.5 to below 9.0, compared to the bulk BR from bare areas. The weathering products, amorphous Fe-Si-Al minerals, were found to have increased in rhizosphere BR samples, as resolved by means of a synchrotron Fe, Al, and Si K-edge near-edge X-ray absorption fine structure spectroscopy (NEXAFS) analysis. These secondary minerals were associated with carboxylic-rich organic molecules derived from root exudates, according to the C 1s NEXAFS analysis. Consequently, the *in situ* inputs of organic carbon from colonizing plants led to a notable increase in total organic carbon from approximately 10 to above 20 $mg \cdot g^{-1}$. These rhizosphere-driven changes seemed to be consistent across plant species, regardless of fertilizer inputs. Therefore, halophytic plant species may be harnessed as biological drivers to initiate early soil formation in BR, where large amounts of organic matter may be infeasible, though this neo-natural soil formation may be a lengthy process.

Keywords: Bauxite residue, Halophytic plants, Dealkalization, Sodalite, Amorphous minerals, Carboxyl groups

Highlights

- Halophytic plant species are important drivers in the weathering of bauxite residue and soil formation under field conditions
- Residual alkaline minerals in BR can be weathered and dealkalized by penetrating roots of halophytic plants.
- Amorphous Fe-Si-Al minerals formed in the rhizosphere are conducive to organo-mineral association and water-stable aggregation.

* Correspondence: Longbin Huang (l.huang@uq.edu.au)

Full list of author information is available at the end of the article.

Graphical abstract

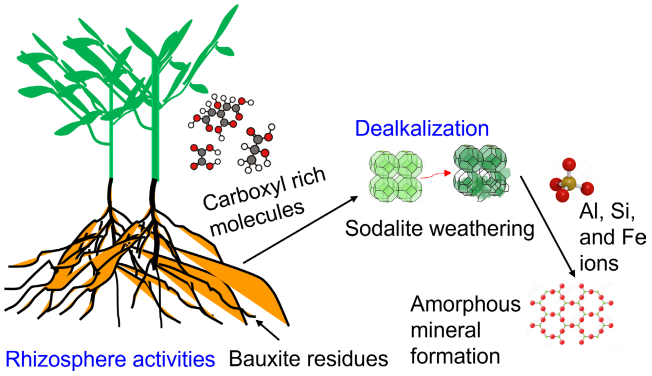

Introduction

The world's aluminum industry is facing the greatest environmental challenge posed by billions of tons of polluting bauxite residue (or red mud) generated from alumina production, which have been stored in purposely constructed storage dams[1]. Eco-engineering of bauxite residue (BR) into soil-like technosol is a promising and cost-effective technology for soilless rehabilitation[2]. The *in situ* eco-engineered soil formation treats BR as parent materials, and employs various eco-engineering inputs such as exogenous organic matter and pioneer plants to accelerate key pedogenetic processes under local climatic conditions, such as mineral weathering and transformation, organo-mineral interactions, and soil physicochemical property development[2]. The extreme alkalinity buffered by alkali-bearing aluminosilicates (e.g., sodalites) is the fundamental barrier to soil formation and sustainable plant growth.

The eco-engineered soil formation in BR emphasizes the acceleration of early soil forming processes, i.e., weathering of alkaline minerals and organo-mineral associations in BR through enhancing the growth and functions of haloalkaliphilic microbes and plants[3–5]. Gypsum/organic approaches have been reported in international literature[6–8]. These studies found that gypsum and/or organic matter inputs can improve physical and chemical conditions of BR and facilitate plant growth. However, when the amendment of large amounts of exogenous organic matter is infeasible, can we harness the rhizosphere power of native plants tolerant to alkalinity and salinity, as biological drivers to initiate mineral weathering and increase *in situ* organic carbon inputs to enhance soil formation in BR?

Pioneer plant species, such as native halophytic plants, are important biological drivers in advancing soil formation from parent minerals in nature, but their roles in initiating alkaline mineral weathering in BR have not been well understood, particularly under field conditions. Halophytes can grow in extremely saline habitats and have developed dual tolerance to salinity and alkalinity[9,10]. Besides, halophytes can synthesize large amounts of organic acids (e.g., acetate, oxalate, formate, lactate) in roots[11]. It is known that tolerant pioneer plant species can colonize partially improved and alkaline Fe-ore tailings, driving mineral weathering and cascaded soil forming processes, such as pH neutralization, geochemical improvement, and water-stable aggregate formation[12,13]. For example, *Atriplex aminocola* (saltbush, a halophyte species) was found to be tolerant to alkaline pH (pH 9.5–10) and high salinity and stimulate biotite-like mineral weathering and secondary amorphous mineral formation in alkaline iron ore tailings[12, 14].

Therefore, halophytes may be introduced as early colonizers to establish an interim vegetation cover for dust suppression and surface erosion control. More importantly, these species could act as biological drivers to initiate the weathering of alkaline minerals and coupled neutralization and rhizosphere organic carbon inputs via root biomass and exudates, as fundamental events in the early BR soil formation. Our previous studies reported the dealkalization of BR minerals by pioneer plants in a pot experiment under glasshouse conditions[15]. The investigation focused on three native halophytes colonizing the surface layer of BR without large amounts of organic matter inputs: saltbush (*Atriplex aminocola*), Rhodes grass (*Chloris gayana*), and Ruby saltbush (*Enchylaena tomentosa var. glabra*), among which the first two species were sown and the last one naturally colonized after three years.

The present study demonstrates field-based evidence about the use of native plants as biological drivers in accelerating mineral weathering and organo-mineral associations, as the early phase of eco-engineered soil formation under field conditions. It has focused on mineral changes in the rhizosphere, particularly, on the key questions: (1) rhizosphere-driven weathering of alkaline minerals and secondary Fe/Al mineral formation in rhizosphere BR, and (2) forms of organics in rhizosphere BR. In nature, phosphorus (P) is acquired by plants in rock-minerals undergoing weathering, but BR is deficient in available P. As a result, phosphate-fertilizer is applied in bauxite residue (BR) to improve available P for plant growth in the present study. Various micro-spectroscopic analysis was used to characterise mineralogical changes by using synchrotron-based X ray diffraction (XRD) and Fe, Al, and Si K edge near edge X-ray absorption fine structure (NEXAFS). The organic carbon forms in rhizosphere BR were determined by the synchrotron-based scanning transmission X ray microscopy (STXM) and C 1s NEXAFS analysis. It is expected that root activities would have stimulated the weathering of sodalite-like minerals in BR, pH neutralization, and the formation of Fe/Al secondary minerals, as they can generate carboxyl rich organic acids in the rhizosphere.

Materials and methods

Field trial and sampling

The field trial was established with air-dry and mechanically ripped seawater-treated bauxite residue (BR) at the Residue Disposal Area (RDA) of Queensland Alumina Ltd (QAL) located in central Queensland, Australia (23.912° S, 151.314° E). The trial plots were fertilised with super-phosphate (super-P) at rates (kg P ha^{-1}) of 0 (nil), 95 (low P), and 250 (high P), which were estimated as equivalent to P fertiliser rates in

the top 10 cm red clay soil for supporting plantation. In the field trial, we introduced salt- and alkaline-tolerant plant species by seed-sowing, in addition to naturally colonizing plant species at the BR treatment plots. After three years of treatments, plants of three different species were not uniformly covering the plots, with some plants at the edge of the BR plots. Some areas of the plots were devoid of plants, which served as bulk areas for comparison. Rhizosphere samples were collected from BR particles adhered to the root system, while bulk samples were collected from the bulk areas without plants. These samples were taken in the vegetative growth season.

Plant species identification was based on morphological characteristics, including observing and analyzing the physical forms of plants, such as leaf shape, flower structure, stem texture, and overall growth form. These characteristics were compared to established botanical descriptions or taxonomic keys to determine the species. Morphological identification relied on standardized criteria within plant taxonomy to ensure accuracy and consistency in classification.

Bulk and rhizosphere samples were sampled in pairs, from three plant species in the BR plots. The samples were categorized into: CK—Bulk samples without plant colonization; SB—Rhizosphere of saltbush (*Atriplex aminocola*); RG—Rhizosphere of Rhodes grass (*Chloris gayana*); RS—Rhizosphere of Ruby saltbush (*Enchylaena tomentosa var. glabra*) (Fig. 1). Bulk BR squares (approximately 15 cm × 15 cm × 25 cm in size) were sampled, containing individual plants together with most roots. Rhizosphere samples were defined as BR particles within approximately 2 mm of root surfaces, which were mostly BR tightly attached to root surfaces. Rhizosphere BR samples were separated from plant roots through gentle shaking (Fig. 1). All samples were freeze-dried before further analysis.

Physicochemical and mineralogical analysis

The pH and electrical conductivity (EC) in 1:5 water extracts were measured using a pH electrode (TPS 900-P), and a EC electrode (TPS 2100), respectively. Total carbon (TC) and total nitrogen (TN) contents in the BR samples were analysed using combustion methods[8]. The freeze-dried and ground BR samples were amended with 10% CaF_2 and subject to quantitative Cu-source X-ray diffraction (qXRD) analysis. XRD spectra were collected at 2θ = 5°–80° with 0.02° per step and processed by Diffrac^{plus} Evaluation Package V5.1 (Bruker D8 DISCOVER diffractometer, Bruker AXS, Germany). The minerals were identified according to the PDF-4 mineral database (2021 release), and quantified by using TOPAS 4.0 (Bruker, Germany).

Synchrotron XRD analyses were carried out at beamline BL01C2, the National Synchrotron Radiation Research Center (NSRRC), Taiwan, China. The XRD spectra were acquired by a large Debye-Scherrer camera with λ = 0.7749 Å (16 keV). The XRD patterns of the samples were obtained using a transmission method. Two-dimensional XRD patterns were captured with a MAR345 imaging plate, and one-dimensional XRD profiles were derived from the 2D data using GSAS-II software. Calibration of geometry and sample position offsets was performed using the NIST standard reference material LaB_6.

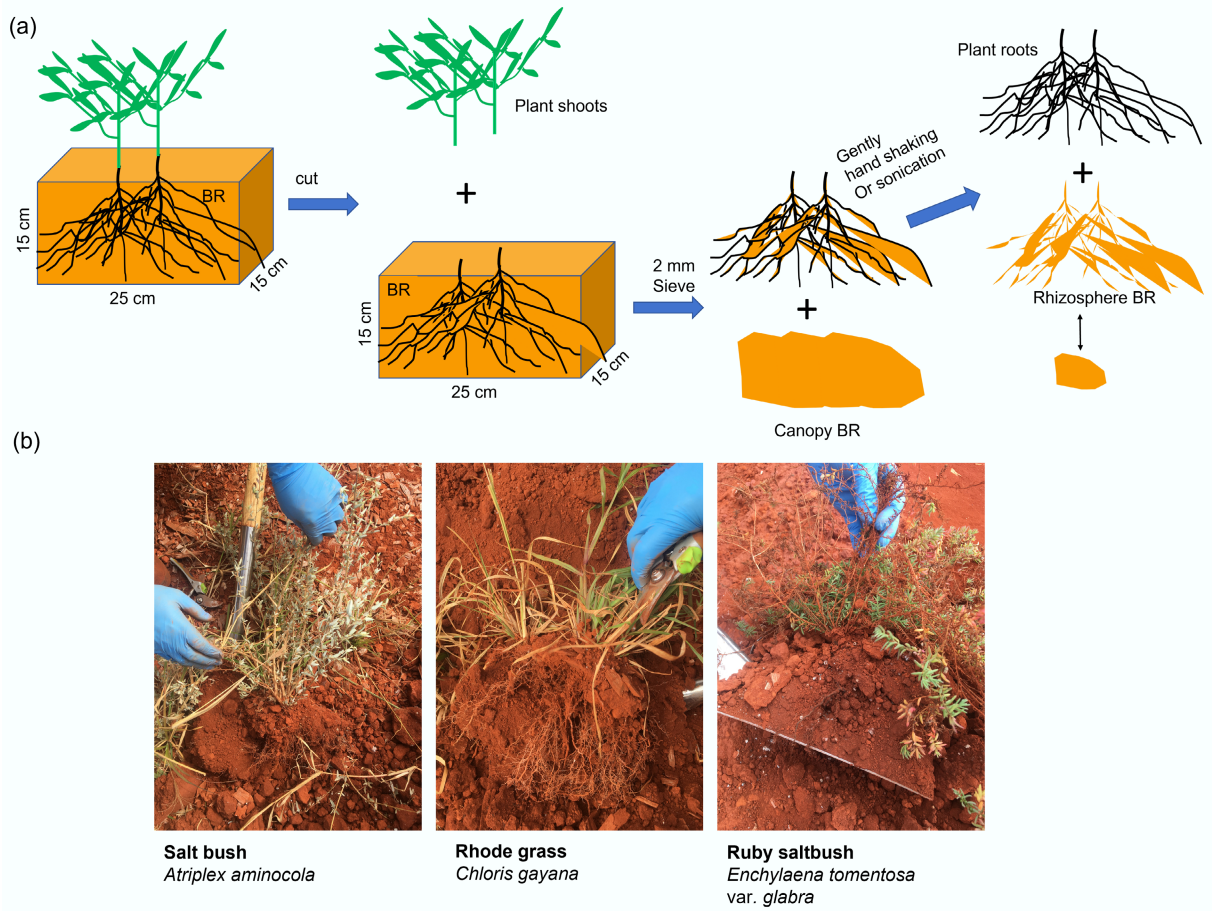

Fig. 1 (**a**) Diagram and (**b**) photos for sampling of rhizosphere bauxite residues in the field. The bauxite residue samples from the rhizosphere of individual plants species were collected, including saltbush (*Atriplex aminocola*), Rhodes grass (*Chloris gayana*), and Ruby saltbush (*Enchylaena tomentosa var. glabra*).

Fe K edge XAFS analysis

Freeze-dried and ground BR samples were subject to Fe K-edge (7,112 eV) XAFS analysis at beamline 01C1 at National Synchrotron Radiation Research Centre (NSRRC), Taiwan, China, to characterize Fe speciation. Fe mineral standards, including biotite, illite, hematite, ferrihydrite, goethite, magnetite, siderite, pyrite, Fe(II) gluconate hydrate, and Fe(III)-oxalate were included. Fe-Si-short range ordered minerals (Fe-Si-SRO) were included to represent Fe-Si-rich amorphous minerals. Phyllosilicates were purchased from Ward's Science (www.wardsci.com), and Fe oxyhydroxides were purchased from Sigma Aldrich. Ferrihydrites were prepared as described previously[16]. Briefly, 40 g $Fe(NO_3)_3{\cdot}9H_2O$ was dissolved in 500 mL MilliQ water with pH adjusted to 7.5 by NaOH. The precipitates were collected through centrifugation, and freeze-drying, confirmed by XRD analysis. The Fe-Si-SRO was synthesized by hydrolysing $Fe(NO_3)_3{\cdot}9H_2O$ in the presence of SiO_3 ligands (Na_2SiO_3) at pH 9 under an atomic Si : Fe ratio of 1[17]. Fe(III)-oxalate complexes were synthesized by mixing Fe(III) solutions ($Fe(NO_3)_3{\cdot}9H_2O$) with oxalic acid at a mole ratio of 1:5.

The Fe K edge XAFS spectra were collected from −200 to 800 eV (relative to the Fe K edge absorption edge of 7,112 eV) under the below energy set: −200 to −20 eV (10 eV/step); −20 to 30 eV (0.35 eV/step); 30 to 800 eV (4 eV/step). The collection time for each step was set to 2 s. The Fe K edge XAFS spectra were collected at transmission mode, with an Fe foil as an internal standard to calibrate the energy. The Fe K edge XAFS spectra were baseline and background corrected and normalized by using ATHENA from DEMETER software package[18]. The k^3 weighted extended X-ray absorption spectra (EXAFS, *k* space from 2.5 to 11.5 $Å^{-1}$) were processed by principal component analysis (PCA). Key Fe standards, including ferrihydrite, hematite, Fe(III)-oxalate, and Fe-Si-SRO were selected for linear combination fitting (LCF) using the ATHENA software package. The total percentage of different Fe phases was not set to 100%, as there may exist other Fe species unidentified in XAFS fitting. The quality control of the LCF fitting was verified by a minimal R-factor.

C, Al, and Si K edge NEXAFS analysis

The synchrotron-based C, Al, and Si K-edge near-edge X-ray absorption fine structure spectroscopy (NEXAFS) analysis was undertaken on the soft X-ray spectroscopy beamline (14ID)[19] at the Australian Synchrotron. The samples were ground and homogenously mounted on copper tape. The synchrotron beam was operated under continuous top-up mode, with a beam size of 1 mm^2. C, Al, and Si K-edge NEXAFS spectra were collected under partial electron yield (PEY) mode at an angle of 55° to the beam. The energy range of the spectra was 270–330 eV for C 1 s NEXAFS with a step size of 0.1 eV and collection time of 0.8 s per step; 1,540–1,620 eV for Al K edge XAFS, with a step size of 0.1 eV and collection time of 0.6 s per step; and 1,820–1,900 eV for Si K edge XAFS, with a step size of 0.2 eV and collection time of 0.6 s per step. Al standards, including sodalite, kaolinite, metakaoline, illite, biotite, and mullite/muscovite, as well as Si standards, including silicic acid, biotite, sodalite, and kaolinite, were analyzed. The spectra were collected with Flood Gun-on mode.

Both Al and Si K-edge NEXAFS spectra data were processed using QANT Igor Pro 8 (WaveMetrics Ltd). The photon energy calibration was performed using the Al standard-single E-aluminum (main peak at 1,566.1 eV) and Si reference standard-single E-silicon (the main peak is 1,843 eV). The monochromator was normalized by aligning it with the simultaneously measured I^0 current (Izero_VF channel) on the sample, to mitigate fluctuations in beam intensity. Then, the background subtraction was normalized by using a linear function of pre- and post-edge in the QANT package. During the normalization, the pre- and post-edge of Al K edge NEXAFS spectra were 1,546–1,554 eV and 1,606–1,614 eV, respectively. The pre- and post-edge of Si K edge NEXAFS spectra were 1,828–1,836 eV, and 1,888–1,896 eV, respectively.

The spectra of C K-edge NEXAFS were analyzed using QANT package (Igor Pro 8 software). The NEXAFS spectra were double normalized by the incident beam (I^0) and a Photodiode Reference scan. Besides, the spectra of highly oriented pyrolytic graphite (HOPG) standard (the main peak is 291.65 eV under exciton mode) were used for energy calibration, which were collected simultaneously with I^0 and the sample's spectra. The background subtraction was processed using a linear function of pre- and post-edge of C 1s NEXAFS spectra –i.e., 272–278 eV, and 323–329 eV, respectively. The peak fitting was conducted using the QANT package[20]. The baseline was set at 290 eV, the edge height was set at 1.3 (a.u.), and the edge width was set at 1.2 eV. The Gaussian peaks at 285.2, 286.8, 287.3, 288.5, 289.3, and 290.3 eV (representing aromatic C, phenolic C, alkyl C, carboxyl C, O-alkyl C, and carbonyl C, respectively) were fitted accordingly. Besides, the peak at ca. 292 eV (1 s → σ* transitions of saturated single covalent bonds[21]) was included in the fitting to enhance the fitting quality. The percentage of a specific organic form was calculated as the quotient of the area of their Gaussian peaks divided by the sum of the areas of all peaks (except the peak at 292 eV)[22].

ATR-FTIR analysis

Functional groups of organic matter or minerals in bulk and rhizosphere BR samples were analyzed by attenuated total reflection Fourier-transform infrared (ATR-FTIR) using a Cary 630 FTIR with Diamond ATR module (Agilent Technologies, Palo Alto, CA, USA). BR samples were thoroughly ground in the agate plates to make sure the particle sizes were below 20 μm. The ATR-FTIR spectra were collected for 400–4,000 cm^{-1} with a resolution of 2 cm^{-1}. The background (i.e., air) was automatically analyzed for baseline correction. The spectra were processed and normalized by Origin 8.5 (OriginLab Corporation, Northampton, MA, USA).

STXM analysis

Scanning transmission X-ray microscopy (STXM) analysis was conducted at the SM beamline within Canadian Light Source (CLS) for the C, N, and mineral distribution in the rhizosphere of SB plants (due to beamtime limited, only rhizosphere SB samples were subjected to STXM analysis). Around 10 mg well-mixed freeze-dried rhizosphere BR sample was suspended in 3 mL MilliQ water, and sonicated for 20 s, then 2 μL suspension was deposited on a Si_3N_4 window and air-dried for STXM analysis. An area of 20 × 15 μm region was scanned with a resolution of 100 nm. The energies of C (1 s edge, with energy range: 280–320 eV), N (1 s edge, 390–450 eV) were collected. The data for C 1 s edge are 280–283 eV at 0.75 eV steps, 283–293.2 eV at 0.15 eV steps, and 293.2–319 eV at 0.5 eV steps. The data for N 1 s edge are 390–398.2 eV at 0.75 eV steps, 398.2–405.2 eV at 0.15 eV steps, 405.0–420.5 eV at 0.75 eV steps, and 420.5–450.0 eV at 1.45 eV steps. The STXM data were processed by Stack_Analyze software within the aXis2000 software package (Hitchcock, A. P. aXis-2000 is an IDL-based analytical package. 2000. http://unicorn.mcmaster.ca)[23]. The stacks were first checked and aligned, and then converted to optical density (OD) following the formula $OD = \ln(I_0/I)$ (I_0 is the incident flux, I is the flux passed through the sample). The mapping of C, N, and minerals were achieved by subtracting the OD in pre-edge from the elemental absorption peak. The C map was based on the signal of the difference between OD value at 288 eV and that at 289 eV; the N map was based on the difference between OD value at 397 eV and that at 402 eV; the mineral distribution map was based on the microscopic identification.

Statistical analysis

The significant differences in pH, EC, TC, and TN concentration among treatments were assessed by one-way ANOVA followed by Tukey's test ($p < 0.05$), using SPSS software package (Ver 27, IBM, Armonk, NY, USA).

Results

Alkaline mineral weathering in bauxite residue subject to root activities

The establishment of halophytic plant species significantly decreased pH in rhizosphere BR from highly alkaline pH > 9.5 to pH 8.5–9.0 ($p < 0.05$) (Fig. 2). Furthermore, the rhizosphere BR had significantly lower EC value to < 3.0 mS cm^{-1}, regardless of the phosphate fertilizer rates ($p < 0.05$). The BR conditions after plant root activities reached the criteria of rehabilitation goals proposed by Di Carlo et al.[24]. Mineralogically speaking, the BR minerals were mainly composed of hematite, sodalite, kaolinite, quartz, gibbsite, boehmite, anatase, rutile, cancrinite, and calcite, as well as 40%–60% of amorphous phases, according to qXRD analysis (Table 1, Supplementary Fig. S1). In rhizosphere BR, the proportion of sodalite was lowered to be < 10% wt%, compared to 10%–14% wt% in the bulk BR, with the lowest in BR associated with RS (Ruby saltbush) roots. The SB (saltbush) and RG (Rhodes grass) colonization also lowered the percentage of hematite from 25%–30% to < 20% in BR amended with high P fertilizer, corresponding with the increase of amorphous phases from 40%–42% to ca. 60%. The synchrotron-based XRD further verified the sodalite weathering in BR modified by halophyte root activities (Fig. 3a), with much lower intensity of sodalite peaks in XRD spectra in rhizosphere BR than in bulk BR (Fig. 3a).

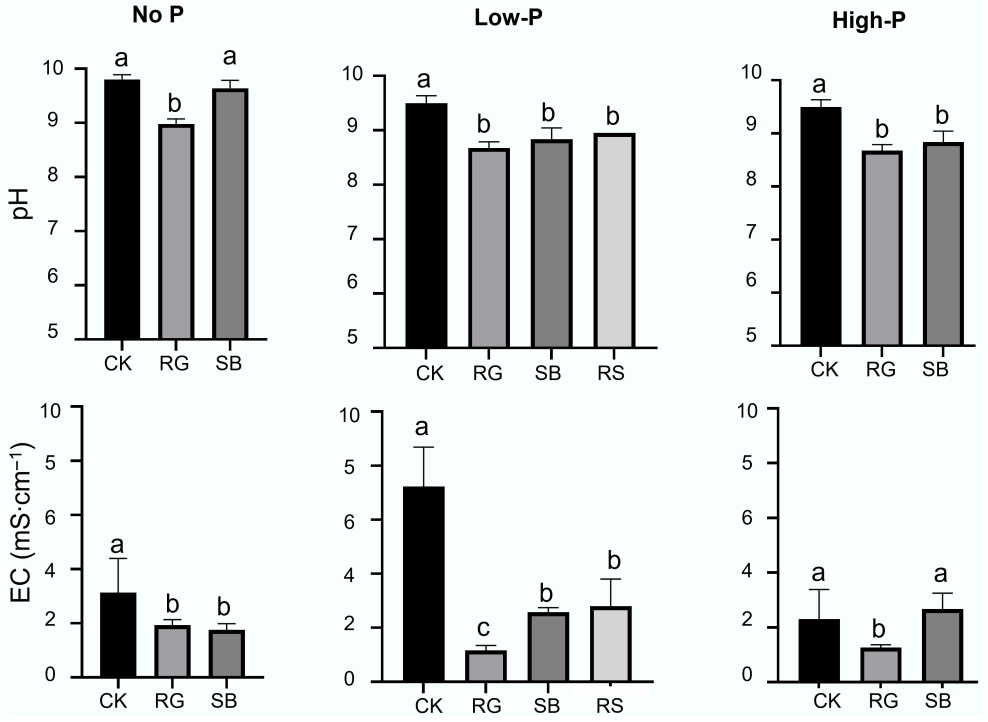

Fig. 2 The pH and electrical conductivity (EC) of bulk and rhizosphere of various plants grown in bauxite residues (BR) in the field trial. Note: CK: bulk samples without plant colonization; SB: rhizosphere of saltbush (*Atriplex aminocola*); RG: rhizosphere of Rhodes grass (*Chloris gayana*)); RS: rhizosphere of Ruby saltbush (*Enchylaena tomentosa* var. *glabra*). 'No P', 'Low P' and 'High P' represent the apply of super-phosphate (super-P) at rates (kg P ha^{-1}) of 0, 95, and 250, respectively. Different letters show significant differences among treatments as revealed by ANOVA followed by Tukey's test ($p < 0.05$, $n = 4$).

Table 1 The mineral phase components (percentage % w/w) in bauxite residues in the field trial

Treatment	Percentage (w%)										
	Gibbsite	Quartz	Boehmite	Anatase	Hematite	Sodalite	Rutile	Kaolinite	Cancrinite	Calcite	Amorphous
CK No P	0.28	1.02	2.48	0.81	21.3	10.6	1.03	1.33	0.59	1.23	59.3
RG No P	0.39	4.98	0.55	0.56	19.3	6.05	1.02	6.79	0.53	0.59	59.3
SB No P	0.25	2.53	0.47	0.75	21.2	6.14	1.03	9.70	0.80	1.02	56.1
CK Low P	0.57	1.83	4.13	0.79	25.8	12.6	1.38	2.88	0.83	0.93	48.2
RG Low P	0.57	4.21	1.10	1.15	26.9	9.35	1.65	9.14	0.63	0.81	44.5
SB Low P	1.14	4.92	0.83	0.78	23.9	8.71	1.13	8.62	0.80	0.68	48.4
RS Low P	0.78	3.45	1.26	0.37	15.6	5.87	0.86	6.65	0.53	0.51	64.1
CK High P	0.38	1.22	4.65	1.07	30.4	14.1	1.39	4.67	0.73	1.33	40.1
RG High P	0.48	2.45	0.53	0.93	19.8	7.02	1.38	6.83	0.18	0.46	59.9
SB High P	0.28	2.19	0.84	0.90	22.6	8.56	1.27	7.85	0.88	0.73	53.9

CK: bulk samples without plant colonization; SB: rhizosphere of saltbush (*Atriplex aminocola*); RG: rhizosphere of Rhodes grass (*Chloris gayana*)); RS: rhizosphere of Ruby saltbush (*Enchylaena tomentosa* var. *glabra*). The treatments 'No P', 'Low P', and 'High P' represent the amendment of super-phosphate (super-P) at rates (kg P/ha) of 0 (No P), 95 (Low P), and 250 (High P), respectively.

Amorphous Al-Si-Fe minerals in BR

Rhizosphere activities of halophytic plants caused the formation of Fe-Si-rich amorphous minerals in BR under field conditions. Synchrotron-based Fe K edge XAFS analysis indicated the presence of amorphous Fe minerals such as Fe-Si-short range ordered (SRO) minerals in rhizosphere BR, compared with bulk BR (Fig. 3b and c). Al K edge NEXAFS analysis revealed peaks at 1,568 and 1,571.5 eV (Fig. 3d), similar to the pattern of the Al atomic environment in illite, or possibly the Al (oxy)hydroxides (broad peak between 1,567–1,571 eV)[25,26]. In Si K edge NEXAFS spectra, there were peaks at 1,848.5 and 1,865 eV, resembling signals of SiO_4^- structure[27,28] and the Si atomic environment in vermiculite or sodalite. The SB (but not the other two species) plant colonization shifted the main peaks of Si K edge XAFS from 1,848.5 to ca 1,849 eV (Fig. 3d), which resembles the main peak of the silicic acid (Supplementary Fig. S2).

Plant root activities induced significant changes in the shape and intensity of ATR-FTIR spectra between 400 cm^{-1} and 1,300 cm^{-1} in BR (Fig. 3e; Supplementary Fig. S3). Regardless of plant species, plant colonization lowered the main peak intensity between 1,200 and 800 cm^{-1} (Supplementary Fig. S3), corresponding to Si-O-Si stretching (around 990 cm^{-1}), and/or inner-surface OH groups of phyllosilicates or Fe-O-Si/Al bonds[29,30]. The rhizosphere BR from RS and RG plants had lower intensity at around 990 cm^{-1} than the SB plant, indicating the reduced Si/Al polymerization in RS and RG colonized BR under low P conditions (Fig. 3e). The peaks between 500 and 750 cm^{-1} in ATR-FTIR spectra were decreased after RS and RG colonization, indicating the diminished Fe-O vibrations from Fe (oxy) hydroxides (Fig. 3e).

Carboxylic-rich molecules in rhizosphere BR

The rhizosphere BR contained higher concentrations of total carbon (TC) than bulk BR (Fig. 4a). SB plant colonization also increased nitrogen (N) concentration in rhizosphere BR (Fig. 4a), but not in rhizosphere BR of RS plants, which contained slightly lower N concentration compared to bulk BR. ATR-FTIR analysis (Supplementary Fig. S3) suggests the likely presence of asymmetric C-H stretch (at around 2,925 cm^{-1}) from aliphatic compounds in both rhizosphere and bulk BR samples. In addition, the rhizosphere BR samples also contained organic molecules exhibiting O-H stretching from phenols or carbohydrates (at around 3,300 cm^{-1}), aromatic/carboxyl/amide (at 1,630 cm^{-1}), and carboxylic or lignin (at 1,380 cm^{-1})[31–33].

Further C forms were characterized by using synchrotron-based C K-edge NEXAFS analysis (Fig. 4b and c). The peaks at 285.2 and 285.5 eV were assigned to aromatic C, 287.6 eV to alkyl C, and around

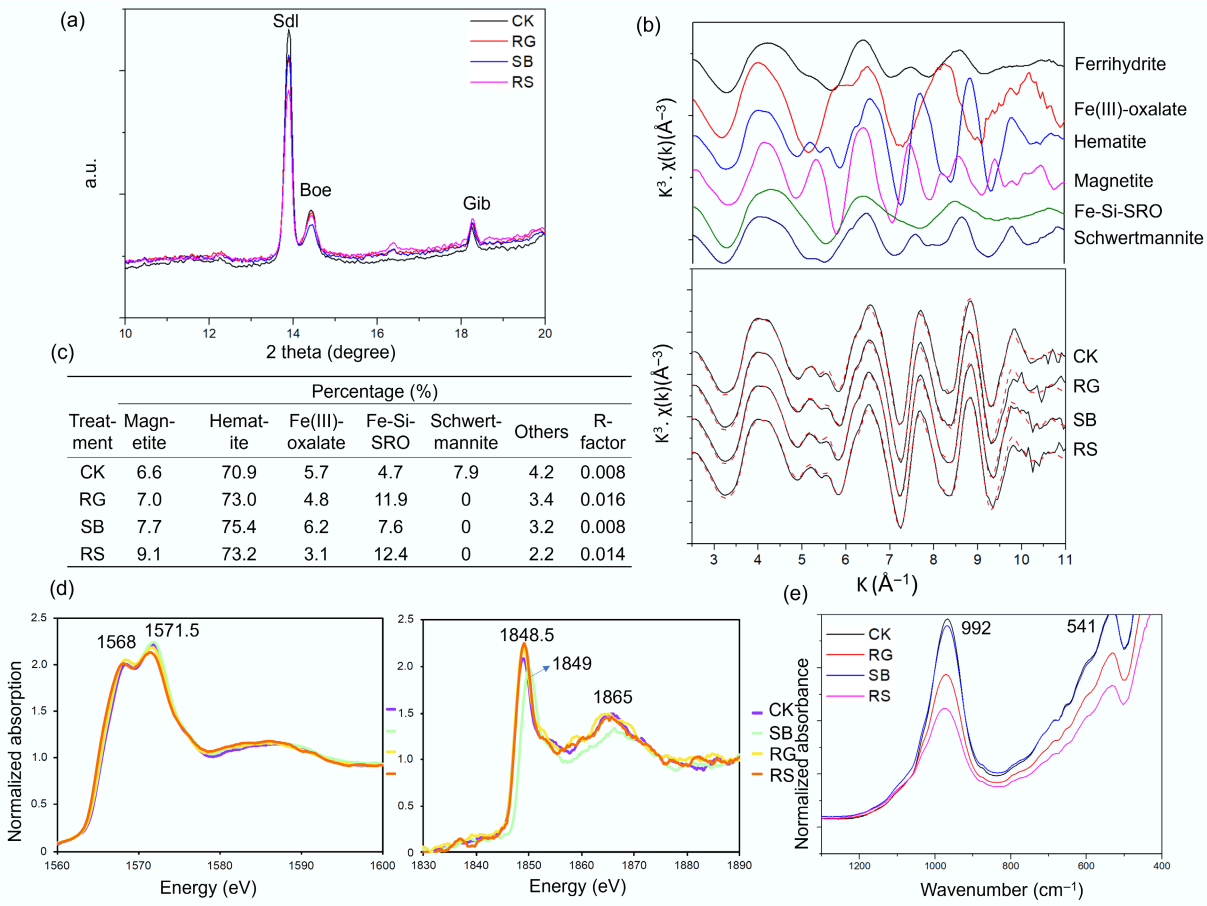

(c)

Treatment	Percentage (%)						
	Magnetite	Hematite	Fe(III)-oxalate	Fe-Si-SRO	Schwertmannite	Others	R-factor
CK	6.6	70.9	5.7	4.7	7.9	4.2	0.008
RG	7.0	73.0	4.8	11.9	0	3.4	0.016
SB	7.7	75.4	6.2	7.6	0	3.2	0.008
RS	9.1	73.2	3.1	12.4	0	2.2	0.014

Fig. 3 Mineral phases in rhizosphere and bulk bauxite residue treated with low rate of superphosphate amendment, as revealed by (**a**) synchrotron-based XRD, (**b**), (**c**) Fe K edge XAFS analysis, (**d**) Al and Si K edge XAFS, and (**e**) ATR-FTIR analysis. In the Fe K edge XAFS analysis, *k* space (k weighted 3) of Fe K-edge EXAFS spectra (line) and linear combination fitting (LCF, dashed) of the Fe phases in the rhizosphere or bulk BR are shown in (**c**). Fe K edge XAFS spectra of several key Fe standards are also presented, including ferrihydrite, Fe-Si-short range ordered (SRO), magnetite, hematite, Fe(III)-oxalate and schwertmannite. Note: Fe(III)-Si-SRO were synthesized by hydrolysing Fe(III) nitrate in the presence of SiO_3 ligands (Na_2SiO_3) at ca. pH = 9. CK: bulk samples without plant colonization; SB: rhizosphere of saltbush (*Atriplex aminocola*); RG: rhizosphere of Rhodes grass (*Chloris gayana*)); RS: rhizosphere of Ruby saltbush (*Enchylaena tomentosa* var. *glabra*).

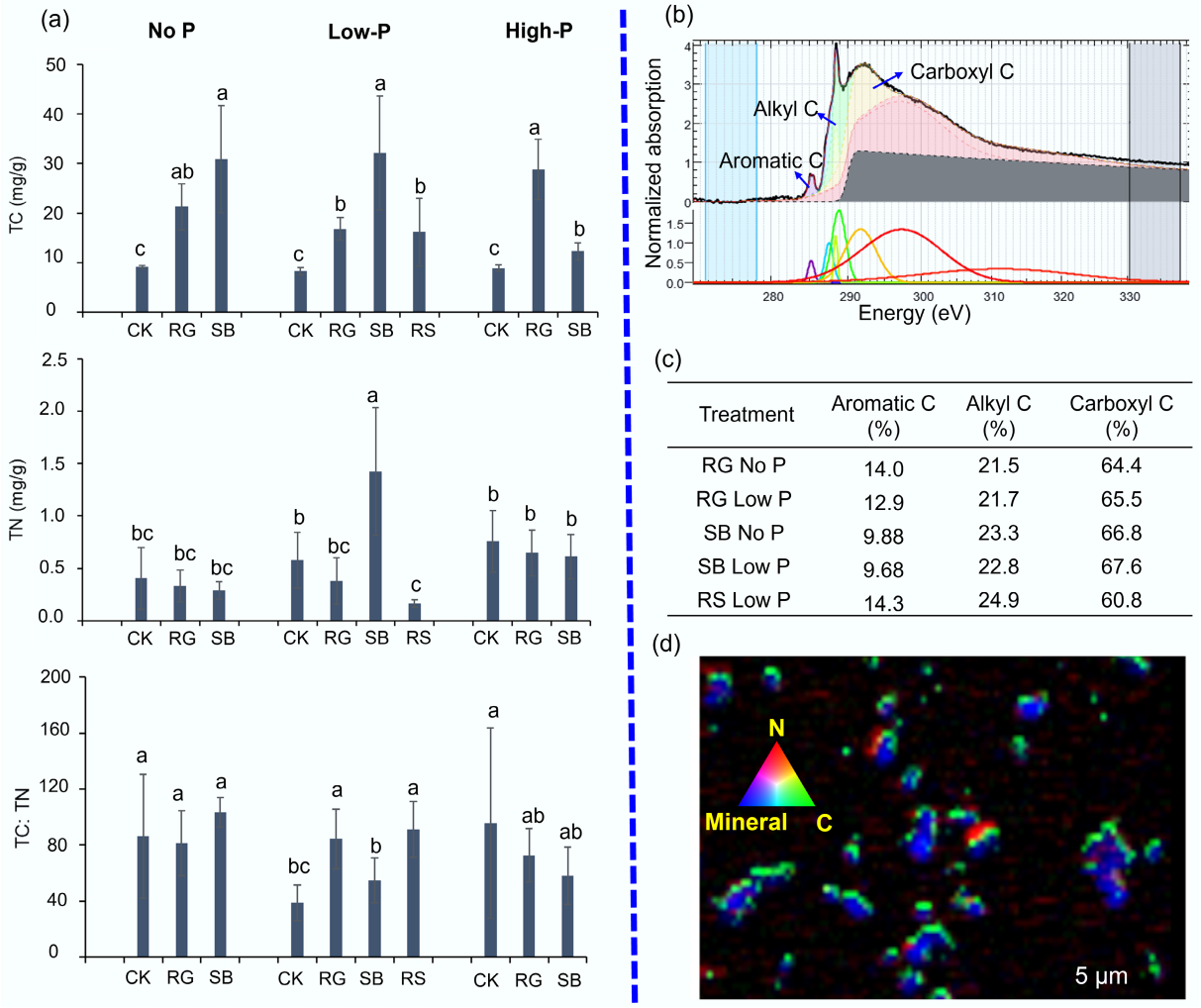

Treatment	Aromatic C (%)	Alkyl C (%)	Carboxyl C (%)
RG No P	14.0	21.5	64.4
RG Low P	12.9	21.7	65.5
SB No P	9.88	23.3	66.8
SB Low P	9.68	22.8	67.6
RS Low P	14.3	24.9	60.8

Fig. 4 Organic carbon chemistry in rhizosphere bauxite residues (BR). (**a**) Total carbon (TC) and total nitrogen (TN) concentration, as well as the TC:TN ratio in rhizosphere and bulk bauxite residue. (**b**), (**c**) Carbon forms in rhizosphere BR as revealed by synchrotron-based C K edge NEXAFS analysis. (**d**) Spatial distribution of C, N, and minerals in the rhizosphere of saltbush (*Atriplex aminocola*) as revealed by synchrotron-based scanning transmission X-ray microscopy (STXM). In (**a**), different letters show significant differences among treatments as revealed by ANOVA followed by Tukey's test ($p < 0.05$). In (**d**), OD values for N, C, and minerals are 0–0.3, 0–3.37, and 0–2.35, respectively. Note: CK: bulk samples without plants; SB: rhizosphere of saltbush; RG: rhizosphere of Rhodes grass; RS: rhizosphere of Ruby saltbush. The treatments 'No P', 'Low P', and 'High P' as in the Materials and methods.

288.9 and 288.4 eV to carboxyl C. The rhizosphere BR samples were enriched mainly with carboxyl C (above 60%), followed by alkyl (ca 20%), and aromatic C (10%). Furthermore, the STXM showed that most of the C and N was tightly associated with minerals in the rhizosphere BR of SB plants (Fig. 4d).

Discussion

The colonization of native halophytic plants induced cascaded changes in mineralogy and geochemistry fundamental to soil formation in BR, such as lowered pH and EC values and reduced proportions of sodalite-like minerals, as well as the increased neoformation of Al-Si-Fe rich amorphous minerals (Table 1, Figs 2 and 3). These may have been caused by root exudation of organic acids, particularly those rich in carboxyl groups (Fig. 4). Organic acids (e.g., low molecular weight organic acids) in root exudates not only lower alkaline pH but enhance mineral weathering through complexing Al and Si from primary alkaline minerals[12, 34]. This organic carbon, derived from rhizosphere activities, is also greatly beneficial to organo-mineral association as the foundation of water-stable aggregate formation towards functional soil construction in BR.

Rhizosphere enhanced weathering of sodalite minerals mediated by organic acids

The halophyte plants decreased pH in BR (Fig. 2), which may be due to the buffering functions of organic exudates derived from root activities. Furthermore, plant colonization also decreased salinity in BR (Fig. 2), which may be because plants take up and accumulate large amounts of Na dissolved from the weathered minerals in rhizosphere BR[35], leading to decreased EC value in the rhizosphere. These improved pH and salinity conditions are beneficial to further colonization of other plant species which may be less tolerant than the native halophytes.

The enhanced weathering of sodalite-like minerals in rhizosphere BR samples may have been caused by biomechanical and biochemical processes of roots[36]. The penetration and expansion of fine roots create close interfaces between root surface and BR minerals, physically breaking down crystalline structure of sodalite[36].

Furthermore, root exudates, particularly those low molecular weight organic acids (LMWOAs), can deform the mineral structure of sodalite cages, and the protons dissociated from organic acids can exchange with the alkali located inside the β-cage of sodalites[37–39]. Besides, root-associated microbial communities in the rhizosphere could also stimulate alkaline mineral weathering through microbial biochemical processes (e.g., generation of acidic metabolites), since halophyte roots could harbour abundant haloalkalitolerant bacteria[40,41].

Although no specific organic molecules were identified in the present study, total carbon (TC) was found to have increased in rhizosphere BR, compared to bulk BR (Fig. 4a). As revealed by ATR-FTIR analysis (Supplementary Fig. S3), those organic molecules in the rhizosphere of BR were mainly comprised of aliphatic compounds, phenols or carbohydrates or lignin. These organic groups may have most likely come from root exudates or root debris of the native halophytic plants. Further speciation of OC forms by means of synchrotron-based C K edge NEXAFS analysis (Fig. 4b and c) identified dominance of carboxyl C (> 60%) groups in the rhizosphere BR, which is indicative of the enrichment of organic acids, most likely coming from root activities (including exudates and biomass debris).

Organic acids can enhance the weathering of aluminosilicate minerals through anionic complexation[39]. Organic complexation with the surface of hydroxysodalite minerals causes hydrolysis of Si–O or Al–O bonds of Si–Al six-membered rings in hydroxysodalite[37]. The silanol or Al–OH groups could be formed as a result of chemical weathering of sodalite[38]. This OC-mineral interaction was verified by the STXM, in which most C was tightly associated with minerals in the rhizosphere of SB plants in BR. Theoretically, organic acids can influence alkaline mineral weathering through the following processes: (1) Organic acids adsorb onto the surface of alkaline minerals; (2) protons from the acids exchange with Na^+ in the crystalline structure of sodalite, reducing the symmetry of the Al-O-Si framework, leading to network hydrolysis; and (3) the conjugate ions of the organic acids chelate with Al and/or Si, altering the coordination environment and promoting the deformation and breakdown of the sodalite structure (i.e., the β-cages)[37,38]. Particularly, the oxygen in the carboxyl groups can act as an electron donor, providing electrons to the empty 3d orbitals of Si and the 3p orbitals of Al, which facilitates the formation of stable organic-Al/Si complexes[42]. Apart from organics-enhanced mineral weathering, these organic molecules have a high affinity to minerals for forming organo-mineral association and soil aggregates.

It is important to note that the percentage of sodalite in BR increased in BR amended with P-fertilizer, which may enhance root system growth and activities, leading to increased sodalite weathering in BR. The P-fertilizer provides phosphate ions (PO_4^{3-}) to the amended BR profile, which may act as a complexing agent to promote the precipitation of aluminosilicate minerals by stabilizing the mineral structure during its formation[43]. In addition, Super-P may have increased soil alkalinity by releasing hydroxide ions (OH^-) or by interacting with other soil components to buffer the pH, creating favourable alkaline conditions for aluminosilicate formation[44].

Formation of amorphous Al-Si-Fe minerals in rhizosphere BR

The generation of amorphous Al-Si-Fe minerals is the consequence of rhizosphere-driven weathering of BR minerals, though there are some background amorphous minerals in BR. According to the synchrotron-based Fe K edge XAFS analysis, amorphous Fe minerals such as Fe-Si-short-range ordered (SRO) minerals were formed in rhizosphere BR, compared to bulk BR (Fig. 3b and c). The enhanced presence of amorphous Fe phases (i.e., Fe-Si-SRO) may be attributed to rhizosphere transformation of minerals[12, 14]. These Fe-Si-SRO minerals may have been formed through the co-precipitation of Fe, Si, and other ions derived from alkaline mineral weathering and Fe mineral transformation[12]. These amorphous Fe minerals could be important sinks for organic matter stabilization in bauxite residues[45].

Furthermore, plant colonization seemed to have lowered the degree of Si/Al polymerization[29], with the strongest effects associated with RS and RG plant species in BR amended with Low P (Fig. 3e). Consequently, amorphous Al-Si-rich minerals might have also been formed in the rhizosphere BR, according to Al and Si K edge NEXAFS analyses (Fig. 3d)[46]. The Al-rich minerals had the patterns of the Al atomic environment in illite or possibly the Al (oxy)hydroxides (broad peak between 1,567–1,571 eV)[25,26], and Si-rich minerals had the structure of SiO_4^-[27,28] similar to the Si atomic environment in vermiculite or sodalite. SB plant colonization may have even led to silicic acid generation in the rhizosphere, as indicated by the shifts of main peaks of Si K edge XAFS from 1,848.5 to ca 1,849 eV (Fig. 3d).

The amorphous silica would interact with Al/Fe-rich minerals in the BR to form Al-Si-Fe-rich amorphous minerals[47,48], as revealed partially by the Fe and Si/Al K-edge XAFS analysis (Fig. 3b–d). This is probably why the intensity of peaks between 500 and 750 cm^{-1}, corresponding to Fe-O vibrations from Fe (oxy)hydroxides, decreased after plant RS and RG colonization in the ATR-FTIR spectra (Fig. 3e). The formation of Al-Si-Fe-rich secondary minerals may result from the combined effects of ion hydrolysis and polymerization[49]. As sodalite dissolves, Si^{4+} and Al^{3+} ions can form negatively charged hydroxy complexes, such as $H_3SiO_4^-$ and $Al(OH)_4^-$, particularly as pH levels rise in BR. These charged species may serve as nucleation centers through electrostatic interactions and hydrogen bonding[50]. Specifically, the strong Lewis acidity of Al^{3+} promotes the creation of Al–O–Si bonds by bridging with silicate ions[51]. The continued deprotonation further facilitated polymerization and build-up of Al-O-Si frameworks with corner-sharing geometry. Furthermore, the presence of Fe^{3+} (from Fe oxyhydroxides in BR), and organic molecules (from root exudates) can hinder Al^{3+} polymerization by introducing structural irregularities or bonding defects, thereby favoring the development of amorphous Al-Si-Fe phases[39, 52]. These Al-Si-Fe- rich amorphous minerals would play an important role in interacting with organics to form organo-mineral association and water-stable aggregates, as the building blocks of soil structure.

Conclusions

This study has among the first to reveal alkaline mineral weathering driven by the rhizosphere of pioneer plants under field conditions. Particularly, through various micro-spectroscopic analyses, we have uncovered the critical processes and mechanisms underlying mineral weathering and organo-mineral association in BR without the initial and once-off capital inputs of organic matter. This study demonstrated that native halophytic plant species can be used as early colonizers in the surface layer of seawater-treated bauxite residue (pH 9.5–10), to initiate alkaline mineral weathering, dealkalization, and *in situ* inputs of organic matter, which led to organo-mineral interactions with amorphous Al-Si-Fe-rich minerals and water-stable aggregates.

These findings provide field-based evidence for understanding the critical role of pioneer plants in early and critical processes of soil formation in BR. Where and when the exogenous organic matter

supply is infeasible under field conditions, tolerant pioneer plant species maybe used as an interim vegetation cover to slowly increased *in situ* OM inputs for initiating soil formation, before eco-engineering rehabilitation could be implemented under field conditions. Nevertheless, it is acknowledged that this plant-based approach without large amounts of inputs of exogenous organic matter in BR can only induce a slow rate of soil formation. It is known that capital inputs of plant biomass organic matter into the profile of the BR matrix would induce an extensive BR modification and cascaded soil formation, due to the much improved physical properties and spatial volumes of root systems in the BR profile (i.e., 50–100 cm). Future studies should focus on the role of pioneer plants in OM-amended BR profiles under field conditions.

Supplementary information

It accompanies this paper at: https://doi.org/10.48130/een-0025-0006.

Ethical statements

The authors declare no ethical issues.

Author contributions

The authors confirm their contributions to the paper as follows: project and research conceptualization, experimental design, funding acquisition: Huang L; methodology, data analysis: Wu S, You F; writing - original draft, Experimental conduction: Wu S; writing - review & editing: Wu S, You F, Parry D, Huang L; critical XRD and XAFS data analysis: Thomsen L. All authors reviewed the results and approved the final version of the manuscript.

Data availability

Supplemental results include XRD, ATR-FTIR, and synchrotron-based Al/Si K edge XAFS analysis. All other data can be requested from the corresponding author.

Acknowledgements

We thank Ms Merinda Hall, Dr Yumei Du, Dr Hao Bu, Mr Chenglong Lu, and Mr Long Ma from the Sustainable Minerals Institute, The University of Queensland for assistance in the sampling and analysis. The C, Al, and Si K edge NEXAFS analysis were conducted by Dr Lars Thomsen on the soft X-ray (SXR) beamline at the Australian Synchrotron (Project reference no. AS223/SXR/18817). We thank Dr Jian Wang from the Canadian Light Source (CLS) for conducting STXM analysis (Project No. GU011781). The authors thanks staff from the Centre for Microscopy and Microanalysis, The University of Queensland, and the Queensland node of the NCRIS-enabled Australian National Fabrication Facility (ANFF) for technical assistance in qXRD and ATR-FTIR analysis.

Funding

This work is financially supported by the Australian Research Council Projects (LP190100975 and DP240102434), Rio Tinto (Aluminum) Ltd, and Queensland Alumina Ltd (QAL).

Declarations

Competing interests

The authors declare that there is no conflict of interest.

Author details

[1]Sustainable Minerals Institute, The University of Queensland, Brisbane, Queensland 4072, Australia; [2]Australian Synchrotron, ANSTO, Melbourne, Victoria 3168, Australia; [3]Rio Tinto, Brisbane, Queensland 4000, Australia

References

[1] Evans K. 2016. The history, challenges, and new developments in the management and use of bauxite residue. *Journal of Sustainable Metallurgy* 2:316–331

[2] Huang L, You F. 2018. Ecological engineering of soil-plant systems to rehabilitate bauxite residues: current progress, barriers and innovations. *Alumina2018 - The 11th AQW International Conference, Gladstone, Queensland, Australia*, ed. Canfell A, Ladhams M. Gladstone, Qld, Australia: AQW Inc. pp. 134–142 https://aqw.com.au/papers/item/ecological-engineering-of-soil-plant-systems-to-rehabilitate-bauxite-residues-current-progress-barriers-and-innovations

[3] You F, Zhang L, Ye J, Huang L. 2019. Microbial decomposition of biomass residues mitigated hydrogeochemical dynamics in strongly alkaline bauxite residues. *Science of The Total Environment* 663:216–226

[4] Ma Y, You F, Parry D, Urban A, Huang L. 2023. Adaptive growth and acidogenic fermentation performance of haloalkaliphilic bacterial communities enriched from biofilms colonising strongly alkaline and saline bauxite residue. *Science of the Total Environment* 856:159131

[5] Di Carlo E, Boullemant A, Courtney R. 2019. A field assessment of bauxite residue rehabilitation strategies. *Science of The Total Environment* 663:915–926

[6] Bray AW, Stewart DI, Courtney R, Rout SP, Humphreys PN, et al. 2018. Sustained bauxite residue rehabilitation with gypsum and organic matter 16 years after initial treatment. *Environmental Science & Technology* 52:152–161

[7] Miura YS, Mulder J, Zivanovic V, Courtney R, Okkenhaug G. 2023. Enhancing bauxite residue properties for plant growth: Gypsum and organic amendment effects on chemical properties of soil and leachate. *Journal of Environmental Management* 337:117721

[8] Wu S, Liu Y, Bougoure JJ, Southam G, Chan TS, et al. 2019. Organic matter amendment and plant colonization drive mineral weathering, organic carbon sequestration, and water-stable aggregation in magnetite fe ore tailings. *Environmental Science & Technology* 53:13720–13731

[9] Flowers TJ, Colmer TD. 2015. Plant salt tolerance: adaptations in halophytes. *Annals of Botany* 115:327–331

[10] Bui E. 2013. Possible role of soil alkalinity in plant breeding for salt-tolerance. *Biology Letters* 9:20130566

[11] Yang C, Guo W, Shi D. 2010. Physiological roles of organic acids in alkali-tolerance of the alkali-tolerant halophyte *Chloris virgata*. *Agronomy Journal* 102:1081–1089

[12] Wu S, Liu Y, Southam G, Robertson LM, Wykes J, et al. 2021. Rhizosphere drives biotite-like mineral weathering and secondary Fe–Si mineral formation in Fe ore tailings. *ACS Earth and Space Chemistry*

[13] Robertson LM, Wu S, You F, Huang L, Southam G, et al. 2020. Geochemical and mineralogical changes in magnetite Fe-ore tailings induced by biomass organic matter amendment. *Science of The Total Environment* 724:138196

[14] Wu S, Liu Y, Southam G, Nguyen TAH, Konhauser KO, et al. 2023. Ecological engineering of iron ore tailings into useable soils for sustainable rehabilitation. *iScience* 26:107102

[15] Lu C, Wu S, Ma L, You F, Saha N, et al. 2025. Haloalkalitolerant plants drive alkaline mineral weathering and dealkalization of seawater-treated bauxite residue. *Plant and Soil*

[16] Schwertmann U, Cornell RM. 2000. *Iron oxides in the laboratory: preparation and characterization*. Winheim, Germany: John Wiley & Sons. doi: 10.1002/9783527613229

[17] Pokrovski GS, Schott J, Farges F, Hazemann JL. 2003. Iron (III)-silica interactions in aqueous solution: insights from X-ray absorption fine

structure spectroscopy. *Geochimica et Cosmochimica Acta* 67:3559–3573

[18] Ravel B, Newville M. 2005. ATHENA, ARTEMIS, HEPHAESTUS: data analysis for X-ray absorption spectroscopy using IFEFFIT. *Journal of Synchrotron Radiation* 12:537–541

[19] Cowie BCC, Tadich A, Thomsen L. 2010. The current performance of the wide range (90–2500 eV) soft X-ray beamline at the Australian synchrotron. *AIP Conference Proceedings* 1234:307–310

[20] Gann E, McNeill CR, Tadich A, Cowie BC, Thomsen L. 2016. Quick AS NEXAFS Tool (QANT): a program for NEXAFS loading and analysis developed at the Australian Synchrotron. *Journal of Synchrotron Radiation* 23:374–380

[21] Solomon D, Lehmann J, Kinyangi J, Liang B, Schäfer T. 2005. Carbon K-edge NEXAFS and FTIR-ATR spectroscopic investigation of organic carbon speciation in soils. *Soil Science Society of America Journal* 69:107–119

[22] Prietzel J, Müller S, Kögel-Knabner I, Thieme J, Jaye C, et al. 2018. Comparison of soil organic carbon speciation using C NEXAFS and CPMAS ^{13}C NMR spectroscopy. *Science of The Total Environment* 628–629:906–918

[23] Hitchcock AP. 2023. Analysis of X-ray images and spectra (aXis2000): a toolkit for the analysis of X-ray spectromicroscopy data. *Journal of Electron Spectroscopy and Related Phenomena* 266:147360

[24] Di Carlo E, Chen CR, Haynes RJ, Phillips IR, Courtney R. 2019. Soil quality and vegetation performance indicators for sustainable rehabilitation of bauxite residue disposal areas: a review. *Soil Research* 57:419

[25] Hu YF, Xu RK, Dynes JJ, Blyth RIR, Yu G, et al. 2008. Coordination nature of aluminum (oxy)hydroxides formed under the influence of tannic acid studied by X-ray absorption spectroscopy. *Geochimica et Cosmochimica Acta* 72:1959–1969

[26] Yoon TH, Johnson SB, Benzerara K, Doyle CS, Tyliszczak T, et al. 2004. *In situ* characterization of aluminum-containing mineral–microorganism aqueous suspensions using scanning transmission X-ray microscopy. *Langmuir* 20:10361–10366

[27] Li D, Bancroft GM, Fleet ME, Feng XH. 1995. Silicon K-edge XANES spectra of silicate minerals. *Physics and Chemistry of Minerals* 22:115–122

[28] Shaw SA, Peak D, Hendry MJ. 2009. Investigation of acidic dissolution of mixed clays between pH 1.0 and −3.0 using Si and Al X-ray absorption near edge structure. *Geochimica et Cosmochimica Acta* 73:4151–4165

[29] Doelsch E, Stone WEE, Petit S, Masion A, Rose J, et al. 2001. Speciation and Crystal Chemistry of Fe(III) Chloride Hydrolyzed in the Presence ofSiO_4 Ligands. 2. Characterization of Si–Fe Aggregates by FTIR and ^{29}Si Solid-State NMR. *Langmuir* 17:1399–1405

[30] Schuttlefield JD, Cox D, Grassian VH. 2007. An investigation of water uptake on clays minerals using ATR-FTIR spectroscopy coupled with quartz crystal microbalance measurements. *Journal of Geophysical Research: Atmospheres* 112:D21303

[31] Chapman SJ, Campbell CD, Fraser AR, Puri G. 2001. FTIR spectroscopy of peat in and bordering Scots pine woodland: relationship with chemical and biological properties. *Soil Biology and Biochemistry* 33:1193–1200

[32] Artz RRE, Chapman SJ, Jean Robertson AH, Potts JM, Laggoun-Défarge F, et al. 2008. FTIR spectroscopy can be used as a screening tool for organic matter quality in regenerating cutover peatlands. *Soil Biology and Biochemistry* 40:515–527

[33] Kenney JPL, Gorzsás A. 2019. Applications of fourier-transform infrared spectroscopy in geomicrobiology. In *Analytical Geomicrobiology: A Handbook of Instrumental Techniques*, ed. Kenney JPL, Veeramani H, Alessi DS. Cambridge: Cambridge University Press. pp. 288–313 doi: 10.1017/9781107707399.012

[34] Drever JI, Stillings LL. 1997. The role of organic acids in mineral weathering. *Colloids and Surfaces A: Physicochemical and Engineering Aspects* 120:167–181

[35] Hasegawa PM. 2013. Sodium (Na^+) homeostasis and salt tolerance of plants. *Environmental and Experimental Botany* 92:19–31

[36] Pawlik Ł, Phillips JD, Šamonil P. 2016. Roots, rock, and regolith: Biomechanical and biochemical weathering by trees and its impact on hillslopes—a critical literature review. *Earth-Science Reviews* 159:142–159

[37] Wang S, Nguyen T, Peng H, Huang L. 2020. On the mechanism of sodic removal from bauxite residue and Bauxite Desilication Products (BDP) using acetic acid. *JOM Journal of the Minerals Metals and Materials Society* 72:309–318

[38] Wang S, Nguyen T, Peng H, Wu S, Parry D, et al. 2023. Sodium removal from bauxite desilication product (sodalite) aided by chelating effects of inorganic and organic acids. *Journal of Environmental Management* 338:117837

[39] Huang PM, Violante A. 1986. Influence of organic acids on crystallization and surface properties of precipitation products of aluminum. In *Interactions of Soil Minerals with Natural Organics and Microbes*. pp. 159–221

[40] Calvaruso C, Turpault MP, Frey-Klett P. 2006. Root-associated bacteria contribute to mineral weathering and to mineral nutrition in trees: a budgeting analysis. *Applied and Environmental Microbiology* 72:1258–1266

[41] Etesami H, Beattie GA. 2018. Mining Halophytes for Plant Growth-Promoting Halotolerant Bacteria to Enhance the Salinity Tolerance of Non-halophytic Crops. *Frontiers in Microbiology* 9:148

[42] Sun XT, Li MR, Xing JT, Li CC, Yuan GH, et al. 2021. The complex effect of organic acids on the dissolution of feldspar at high temperature. *Environmental Earth Sciences* 80:244

[43] Reed T, Mauro JC, Gevaudan JP. 2024. Influence of phosphates on phase formation in alkali-activated MgO-Al_2O_3-SiO_2-P_2O_5 cements. *International Journal of Ceramic Engineering & Science* 6:e10232

[44] Ocanto F, Álvarez R, Urbina De Navarro C, Lieb A, et al. 2008. Influence of the alkalinity and NO_3^-/Cl^- anionic composition on the synthesis of the cancrinite–sodalite system. *Microporous and Mesoporous Materials* 116:318–322

[45] Wu S, Konhauser KO, Chen B, Huang L. 2023. "Reactive Mineral Sink" drives soil organic matter dynamics and stabilization. *NPJ Materials Sustainability* 1:3

[46] Ildefonse P, Cabaret D, Sainctavit P, Calas G, Flank AM, et al. 1998. Aluminium X-ray absorption Near Edge Structure in model compounds and Earth's surface minerals. *Physics and Chemistry of Minerals* 25:112–121

[47] Swedlund PJ, Miskelly GM, McQuillan AJ. 2010. Silicic acid adsorption and oligomerization at the ferrihydrite–water interface: interpretation of ATR-IR spectra based on a model surface structure. *Langmuir* 26:3394–3401

[48] Kanematsu M, Waychunas GA, Boily JF. 2018. Silicate Binding and Precipitation on Iron Oxyhydroxides. *Environmental Science & Technology* 52:1827–1833

[49] Bi S, Wang C, Cao Q, Zhang C. 2004. Studies on the mechanism of hydrolysis and polymerization of aluminum salts in aqueous solution: correlations between the "Core-links" model and "Cage-like" Keggin-Al13 model. *Coordination Chemistry Reviews* 248:441–455

[50] Jun YS, Kim D, Neil CW. 2016. Heterogeneous nucleation and growth of nanoparticles at environmental interfaces. *Accounts of Chemical Research* 49:1681–1690

[51] Hensen EJM, Poduval DG, Magusin PCMM, Coumans AE, van Veen JAR. 2010. Formation of acid sites in amorphous silica-alumina. *Journal of Catalysis* 269:201–218

[52] Nail SL, White JL, Hem SL. 1976. Structure of aluminum hydroxide gel I: initial precipitate. *Journal of Pharmaceutical Sciences* 65:1188–1191